



Pergamon

Acta Materialia 50 (2002) 2613–2625



www.actamat-journals.com

Cracking in brittle laminates from concentrated loads

Herzl Chai [☆], Brian R. Lawn ^{*}

Materials Science and Engineering Laboratory, National Institute of Standards and Technology, Gaithersburg, MD 20899-8500, USA

Received 3 December 2001; received in revised form 18 February 2002; accepted 13 March 2002

Abstract

A study is made of the crack resistance of multilaminates consisting of brittle layers interleaved with compliant interlayers and bonded to compliant substrates. Specific attention is paid to flexure-generated radial cracks in the undersurfaces of individual glass layers from concentrated loads applied at the top surfaces. A proposed condition for acceptance of such multilayer systems is that radial cracking in the upper layers should not occur before analogous radial cracking at the undersurface of an equivalent monolithic coating. Model multilayer systems constructed from glass plates laminated with polycarbonate interlayers and glued onto a polycarbonate base are used to test this condition. These systems enable in situ viewing of radial cracks through polished side surfaces. Critical loads to initiate such radial cracks are measured for multilayers with selected numbers of layers and interlayer/glass thickness ratios. Simple, approximate, semi-empirical closed-form relations are derived for the critical loads, and validated against predictions from finite element computations. We demonstrate the general existence of optimum conditions for multilayer design in terms of numbers of brittle layers, ratios of adhesive interlayer to brittle layer thickness, and modulus mismatch ratios. Published by Elsevier Science Ltd on behalf of Acta Materialia Inc.

Keywords: Brittle layers; Concentrated loads; Design diagrams; Multilayers; Radial cracks

1. Introduction

Studies have recently been made of bilayers consisting of hard, brittle monolithic coating layers on soft, tough substrates, using glass/polycarbonate as a model system for in situ viewing of crack

initiation and evolution in contact loading [1,2]. In such structures the stiff outer layers absorb the bulk of the externally applied loads and “protect” the soft underlayers. The soft underlayers in turn prevent the spread of any cracks into the interior. Most dangerous are radial cracks that originate at the coating undersurfaces, from flexure of the coating on the compliant substrate. Radial cracks can occur at relatively low loads, especially in thinner coatings, and can extend over long lateral distances, ultimately contributing to delamination and failure. Explicit analytical relations for the critical loads required to initiate radial cracks have been established, in terms of basic material properties and

^{*} Corresponding author.

E-mail address: brian.lawn@nist.gov (B.R. Lawn).

[☆] Guest scientist, on leave from the Department of Solid Mechanics, Materials and Systems, Faculty of Engineering, Tel Aviv University, Tel Aviv, Israel.

Information on product names and suppliers in this paper is not to imply endorsement by NIST

coating thickness, using solutions for beams and plates on soft foundations [1,3,4].

The question arises: can further benefit be realized by replacing a monolith coating of thickness D with a laminate of n brittle layers each of thickness $d=D/n$, bonded together with soft adhesive interlayers of thickness $h<d$? In one extension of the above glass/polycarbonate studies [5], replacement of the single glass layer by a glass/sapphire bilayer markedly reduced the susceptibility to radial fracture in the outer glass, by transferring the stress to the stiffer inner sapphire (although the sapphire itself became susceptible to fracture). An important functional advantage of multilayers is that any such cracking may be contained within an individual brittle layer, further confining the spread of damage. This is the principle of damage tolerance. However, brittle multilayer coatings consisting of like stacked plates may be subject to premature failure in thin upper members at relatively low loads, owing to enhanced flexure of those layers on the bonding adhesive [2]. The danger is that radial cracking may occur at a much lower critical load P_1 in the undersurface of layer 1 than the corresponding critical load P_n in layer n , leading to premature failure. For such a system to be acceptable, it is necessary to ensure that $P_1/P_n \geq 1$.

Several practical applications may be cited as motivating forces for the study of brittle multilayers on soft substrates. Dental crowns [6,7] and total hip replacements [8] are important biomechanical examples. Engineering applications include glass-polymer laminates for protective windows [9–13], thermal barrier coatings [14], and hard disk drives for computers [15]. Precedents for the kind of multilayer systems under consideration here exist in the materials engineering literature: laminar zirconia [16] and silicon nitride [17] composites; ceramic/metal multilayers [18]; and carbon fiber cross-ply composites [19]. All of these systems show some form of distributed damage rather than single brittle crack failure. However, little attention has been paid to quantification of the critical loads for first damage which, in many applications (especially biomechanical), signals the end of usefulness of the structure [3].

In this paper we examine the response of model multilayer systems to concentrated loads, follow-

ing the procedure previously used to study bilayers [1,2]. Glass plates of fixed thicknesses are laminated with polycarbonate sheet interlayers, all bonded together with a thin layer of epoxy adhesive onto a polycarbonate base. Such systems allow for in situ viewing of radial crack evolution in individual plates through polished side surfaces, as well as from below. An added advantage of glass as a model brittle material is the ability to control the bulk material strength by abrading or etching one or all of the undersurfaces, to facilitate selective examination of radial cracking in any prescribed layer. Critical loads to initiate radial cracks in each such layer are measured for multilayers with selected numbers of layers n and interlayer/glass thickness ratios h/d . Analytical relations for these critical loads using modified forms of earlier bilayer relations are presented, and validated against predictions from finite element computations for selected hypothetical multilayer systems. We demonstrate the existence of optimum conditions for layer design in terms of numbers of layers, ratios of adhesive interlayer to brittle layer thickness, and modulus mismatch factors.

2. Radial crack patterns in multilayers

2.1. Statement of problem

Consider a laminate with n individual brittle ceramic layers of thickness d and modulus E_c , alternating with thinner interlayers of thickness h ($h<d$) and low modulus E_i ($E_i < E_c$), with the whole bonded onto a comparatively thick substrate of low modulus E_s ($E_s < E_c$), Fig. 1. Suppose the multilayer to be subjected to a concentrated force P by a spherical indenter at its top surface; and let the sphere radius r be sufficiently small that the contact radius can be considered negligible relative to the coating layer thickness, i.e. equivalent to a point load (conservative design). Then, provided none of the constituent layers undergoes inelastic deformation, a linear relation exists between load and stress at any point, enabling certain simplifications in analysis. The potential advantage of the laminate is that the softer interlayers may contain any cracking within a single brittle layer. The danger is that

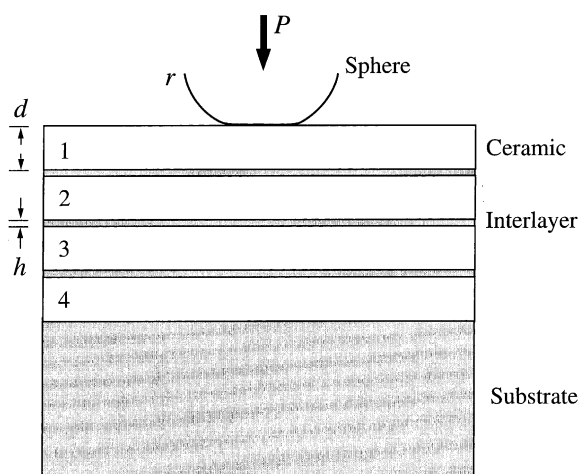


Fig. 1. Schematic showing laminate of $n=4$ layers each with thickness d bonded with compliant interlayer of thickness h , the whole bonded in turn onto a compliant substrate, in contact with sphere at load P at the top surface.

radial cracking may occur at a much lower critical load in the undersurface of the top brittle layer, or indeed in any one of the $n-1$ top layers, relative to that in the undersurface of a monolayer of equivalent net thickness $D=nd$. The paramount question becomes: can we design the multilayer to avert this danger, i.e. maintaining $P_i < P_n$ ($i=1, 2, \dots, n-1$), thereby ensuring superior structural performance?

2.2. Experimental observations of radial crack evolution

Simple multilayers were fabricated from stacks of $n=2, 3$ and 4 soda-lime glass microscope slides (Fischer Premium, Fischer Scientific, Pittsburgh, PA), each of fixed thickness $d=1.0$ mm and surface dimensions $75 \text{ mm} \times 25 \text{ mm}$. Undersurfaces of selected slides in the multilayer sequences were preabraded with 600 SiC grit to provide controlled starting flaws for subsequent radial crack initiation [1,2]. Independent four-point flexure tests on individual abraded glass slides gave reproducible strengths, $\sigma_F=125 \pm 7$ MPa. All other glass undersurfaces were etched in hydrofluoric acid (12% HF for 2 min), to minimize radial cracking in other than specified layers. The top glass surface was similarly etched, to minimize cone cracks.

Polycarbonate sheets of prescribed thicknesses (Hyzod, AIN Plastics, Norfolk, VA) were inserted between adjacent glass slides and bonded with a thin layer of epoxy adhesive (Harcos Chemicals, Bellesville, NJ) to form compliant interlayers of net thicknesses $h < d$. (Because the adhesive has similar mechanical properties to those of the polycarbonate sheet, the interlayers could be regarded as effectively homogeneous through the thickness h [1].) In some cases the polycarbonate sheets were omitted, to produce very thin interlayers ($h < 10 \mu\text{m}$). The same epoxy was used to bond the resulting multilayers to thick (12.5 mm) polycarbonate substrates.

The specimens were indented with tungsten carbide (WC) spheres (J & L Industrial, Livonia, MI), radius $r=3.96$ mm, mounted into the crosshead of a testing machine (Instron Model 4501, Instron Corp, Canton MA). Indentations were made at constant crosshead speed $0.5 \text{ mm} \cdot \text{min}^{-1}$, in air. The evolution of any radial (and/or cone) cracking in the glass was observed through polished side walls (or from below through the substrate) using an optical zoom system (Optem, Santa Clara, CA) mounted into a video camcorder (Canon XL1, Canon, Lake Success, NY). Critical loads P_i for radial fracture in any i^{th} glass layer ($i=1, 2, 3, \dots, n$) were measured as a function of n and h . Several indentation tests could be made on any one specimen surface.

A micrograph sequence for one specific multilayer system with $n=4$ layers, glass thickness $d=1.0$ mm and interlayer thickness $h=280 \mu\text{m}$, is shown in Fig. 2. In this specimen all the glass undersurfaces were preabraded, so as to reveal the succession of cracking through the multilayer at increasing loads. Radial cracking appears first in the top layer (Fig. 2a) at load $P_1 \approx 230$ N, followed by sequential cracking at $P_2 \approx 850$ N (Fig. 2b), $P_3 \approx 1320$ N (Fig. 2c) and $P_4 \approx 1370$ N (Fig. 2d). In all layers the radial cracking was marked by a distinct pop-in event. With increasing load, several radial cracks developed in each layer (as confirmed from subsurface viewing [1,2])—some of these cracks are inclined to the plane of the figure, and are not readily visible in the side views. (Note that a cone crack has initiated between Fig. 2a and b, suggesting that the contact itself may have intro-

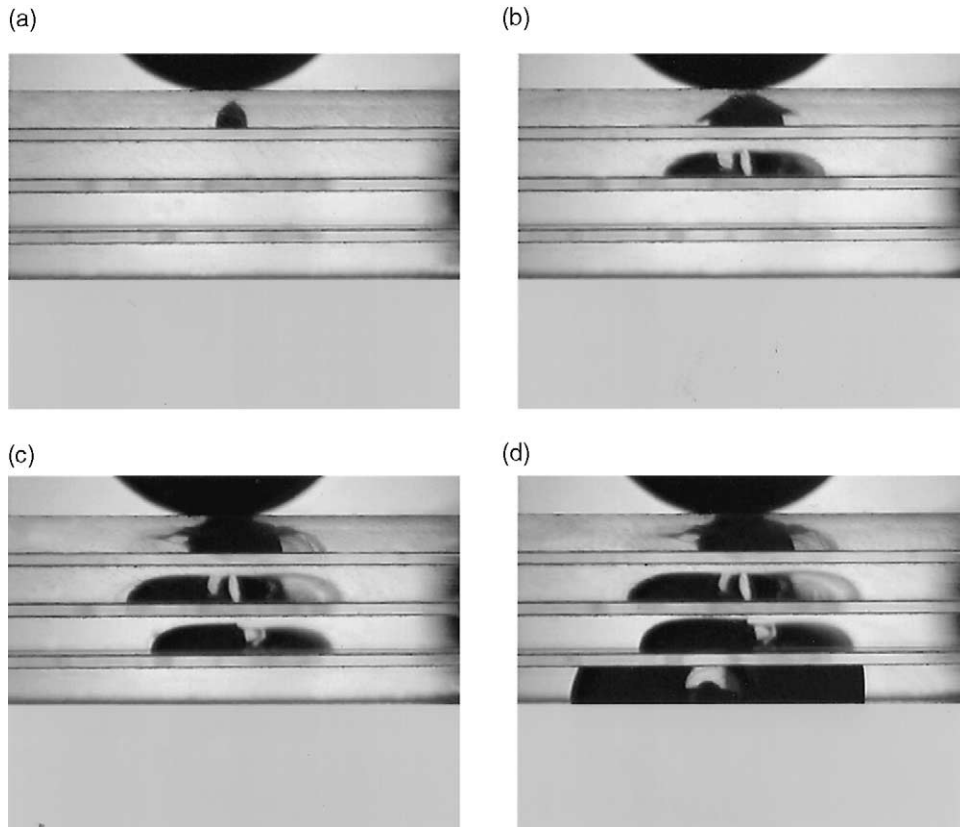


Fig. 2. Micrograph sequence for glass/polycarbonate laminate on polycarbonate substrates, $d=1.0$ mm, interlayer thickness $h=280$ μm , showing radial cracks in individual glass layers. Load sequence (a) $P=230$ N, (b) $P=850$ N, (c) $P=1320$ N, (d) $P=1370$ N. All glass undersurfaces preabraded. (Note appearance of cone crack in the glass top layer in b.)

duced surface flaws into the etched glass top surface.) The radial cracks remain confined within each of the three top layers over the load range, but penetrate through to the opposite surface in the bottom layer. At this last stage the structure is at the point of delamination at the weak interlayer interfaces, and hence total failure. The damage tolerance is evident in the broad load range between the first and last cracks, $P_4/P_1 \approx 6$.

Fig. 3 is a micrograph illustrating the response in a comparative experiment with the same preabraded glass slides but with a much smaller interlayer thickness $h=28$ μm . Again, radial cracking occurred first in the top layer, at $P_1 \approx 560$ N, but in this example virtually simultaneously in the remaining layers, at $P_2 \approx P_3 \approx P_4 \approx 1400$ N. Note that the critical load $P_4 \approx 1400$ N for cracking in

the bottom layer is similar in Figs. 2 and 3. Further experiments with interlayer thicknesses down to $h < 10$ μm showed a similar sequence of events, but with progressively increasing critical load P_1 in the top layer. In principle, we should ultimately expect a reversal in the fracture sequence as $h/d \rightarrow 0$ (monolith limit), so that $P_1 > P_4$. Although we were unable to observe this load-reversal condition in our multilayers, even down to the minimum achievable epoxy interlayer thicknesses ($h \approx 3$ μm), we shall demonstrate below that circumstances can exist where such a condition is indeed achievable.

2.3. Finite element analysis

Finite element analysis (FEA) was used to evaluate stress distributions in the multilayer struc-

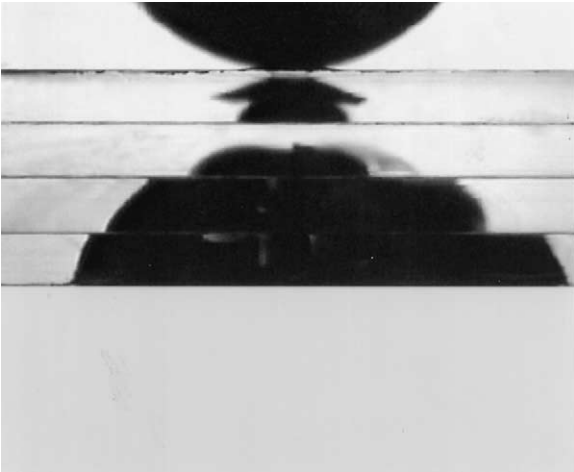


Fig. 3. Same as Fig. 2, but interlayer thickness $h=28\text{ }\mu\text{m}$, load $P=1400\text{ N}$. Radial cracking appeared first in glass layer 1 at $P=560\text{ N}$, in remaining glass layers virtually simultaneously at $P=1400\text{ N}$. (Again, note appearance of spurious cone crack.)

tures in axisymmetric contact loading. The algorithm used here was analogous to that in preceding studies on layer structures [1,5,20], except that the computations were carried out with ANSYS software (Version 5.4, ANSYS Inc., Cannonsburg, PA). The system was configured to load a frictionless WC sphere of specified radius r onto the specimen top surface. All components in the structure were assumed to deform elastically, and the interfaces were assumed to be well bonded. The specimen radius was twice the total specimen thickness. Grid spacings were refined until convergence was attained in test runs, with more than 10^4 total elements and at least 40 through-thickness elements in any one glass plate and six such elements in the intervening layers.

Our interest lies primarily in the tensile stresses at the bottom surface of the brittle layers, where the radial cracks initiate. As an illustrative case study, we choose a configuration pertinent to the glass/polycarbonate system in Fig. 2, i.e. with relatively thick interlayers. Input parameters are as follows: *number of layers*, $n=4$; *glass layers*—thickness $d=1.0\text{ mm}$, Young's modulus $E_g=70\text{ GPa}$ and Poisson's ratio $\nu_g=0.22$; *polycarbonate substrate*—thickness 12.5 mm , $E_s=2.35\text{ GPa}$ and $\nu_s=0.41$; *interlayers*—thickness $h=280\text{ }\mu\text{m}$, $E_i=2.35\text{ GPa}$ and $\nu_i=0.41$ (i.e. same as substrate); *sphere*, radius

$r=3.96\text{ mm}$, $E_i=614\text{ GPa}$ and $\nu_i=0.22$. A contour plot of the hoop tensile stresses [1] is shown in Fig. 4, using an intermediate contact load $P=1000\text{ N}$. The vital role of the interlayers in shielding the lower layers by disrupting the stress distributions is evident. In this example the relatively thick interlayers ($h/d=0.28$) allow substantial flexure of the overlying glass layers, evidenced by the flattened contours in the lower layers, with resultant high tensile stresses σ_i at the undersurfaces. In the top surface of the first glass layer, flexure stresses are dominated by local Hertzian contact stresses

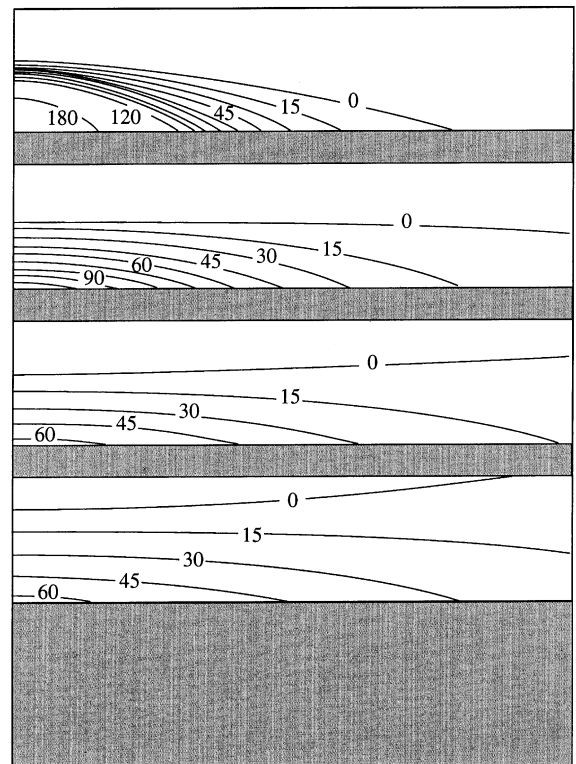


Fig. 4. FEA contour plots for glass/polycarbonate laminates on polycarbonate substrates showing hoop tensile stresses (MPa) in multilayers from contact with sphere indenter at load $P=1000\text{ N}$, for $n=4$. Adhesive interlayers of thickness $h=280\text{ }\mu\text{m}$, elastic parameters $E_i=2.35\text{ GPa}$ and $\nu_i=0.41$. Other material input parameters: *sphere*, $r=0.5\text{ mm}$, $E_i=614\text{ GPa}$ and $\nu_i=0.22$ (contact radius 0.44 mm , not shown); *brittle layers*, $d=1.0\text{ mm}$, $E_g=70\text{ GPa}$ and $\nu_g=0.22$; *substrate* (thickness 12.5 mm , not wholly shown), $E_s=2.35\text{ GPa}$ and $\nu_s=0.41$. Contours in increments of 15 MPa . (Only half-laminate shown. Stresses in interlayers and substrate not shown.)

(responsible for the cone cracks observed in Fig. 2). The magnitudes of the maximum undersurface stresses follow the sequence $\sigma_1 > \sigma_2 > \sigma_3 > \sigma_4$, consistent with $P_1 < P_2 < P_3 < P_4$ in Fig. 2.

Fig. 5 shows a comparative contour plot for the same glass/polycarbonate system at the same contact load $P=1000$ N but with relatively thin interlayers, $h=28$ μm , pertinent to Fig. 3. The level of stress σ_1 at the top layer undersurface is now much less intense than in the corresponding layer in Fig. 4, attributable to substantially reduced plate flexure. This translates into a higher predicted value for P_1 , consistent with observations in Fig. 3 relative to Fig. 2. In the lower layers, the stress contours become nearly continuous across the interfaces, indicating a much reduced shielding effect. Again, this is consistent with the observed condition $P_2 \approx P_3 \approx P_4$ in Fig. 3. Note that the maximum tensile stress σ_4 at the lowest brittle undersurface of Fig. 5 is approximately the same as in Fig. 4,

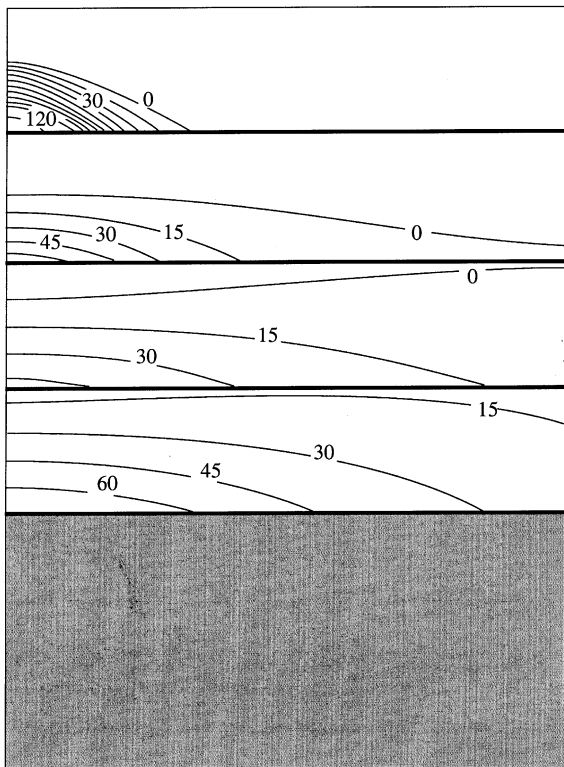


Fig. 5. Same as Fig. 4, but for adhesive interlayers of thickness $h=28$ μm .

indicating that the upper interlayers do little to shield the tensile stress at the bottom of the multilayer from the contact load.

3. Analysis of experimental critical load data

Using the experimental setup in Sect. 2.2., critical loads P_i for radial crack initiation in glass/polycarbonate multilayers with $n=1-4$ layers were measured in situ, for specimens with fixed glass thickness $d=1.0$ mm and sphere radius $r=3.96$ mm, and for different interlayer thicknesses h . In these experiments only one glass undersurface was abraded in each specimen, so that the P_i values could be determined independently. At least five indentations were made at each condition, to determine means and standard deviation error bounds. The FEA algorithm in Sect. 2.3. was then used to validate the data trends, by incrementing the contact load until the maximum tensile stress at the appropriate i th glass undersurface equalled the bulk strength $\sigma_F=125$ MPa of the abraded glass, thereby identifying the critical loads P_i .

Fig. 6 shows critical load data P_i as function of i ($i=1, 2, \dots, n$; $n=1, 2, 3, 4$), for fixed $h=280$ μm .

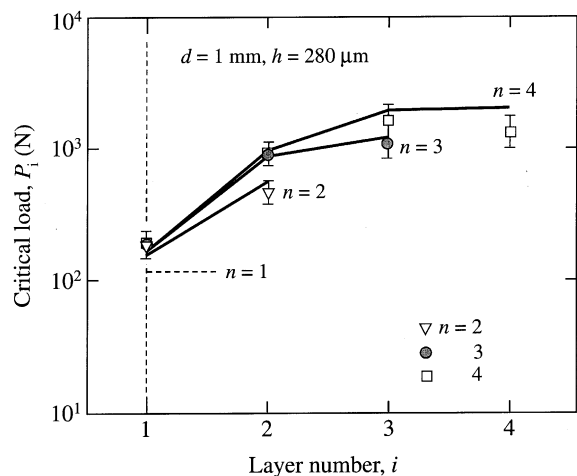


Fig. 6. Critical loads $P_i(i)$ for radial cracking in glass/polycarbonate laminates on polycarbonate substrates, for $n=1-4$, $h=280$ μm , $d=1.0$ mm, $r=3.96$ mm. Each i th glass undersurface selectively preabraded. Data points are experimental means and standard deviations, solid lines are FEA predictions, dashed line at $n=1$ is bilayer baseline.

Solid lines are FEA predictions (note that only integer values of i are allowable). In this system $P_1 < P_i$ for all $i > 1$, consistent with dominant flexure of the top glass layer on the immediate compliant interlayer. The value of P_1 for $n > 2$ is somewhat higher than for $n=1$ (reference bilayer), confirming a supportive role of the glass sublayers [2]. Note, however, that the addition of layers beyond $n=2$ has relatively little effect on P_1 , so most of the support comes from the glass sublayer $i=2$. For $n=4$, the critical loads follow the sequence $P_1 < P_2 < P_3 \approx P_4$, consistent with the trends in Figs. 2 and 3. Note also that the critical load $P_4=1400$ N in Fig. 6 (only layer $n=4$ abraded) is similar to that in Figs. 2 and 3 (all layers abraded), even though cracking in the latter case occurred first in the upper layers at much lower loads, suggesting that the any fractures in the first layers do not seriously degrade the final load bearing capacity of the laminate.

Fig. 7 shows critical load data P_1 for top layer cracking as a function of interlayer thickness h , for all model multilayers ($n=1-4$). Again, the solid curves are FEA predictions. Values of P_1 for multilayers ($n > 1$) lie well above the bilayer baseline ($n=1$) at 115 N, the more so at low h . (P_1 for refer-

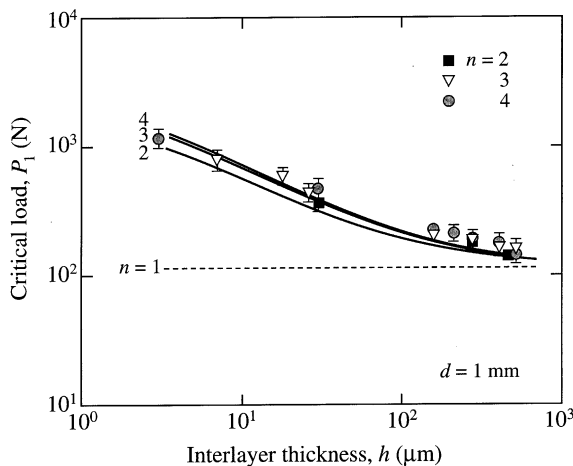


Fig. 7. Critical loads $P_1(h)$ for top layer radial cracking in glass/polycarbonate laminates on polycarbonate substrates, for $n=1-4$, $d=1.0$ mm, $r=3.96$ mm. Undersurface of top glass layer preabraded. Data points are experimental means and standard deviations, solid curves are FEA predictions, dashed line at $n=1$ is bilayer baseline.

ence bilayers is independent of h because of the similarity in interlayer and substrate properties.) Once more, the addition of layers beyond $n=2$ does not substantially influence P_1 . All data converge to the bilayer limit at $h \approx d=1$ mm, as may be expected [2].

From these figures we may conclude that the FEA algorithm is able to predict essential data trends, within experimental scatter bounds.

4. Analytical relations for critical loads

Although FEA is ideally suited to determination of stress distributions in complex multilayer structures, it is limited to case-by-case studies. Closed-form analytical relations, where practical, are a more powerful means of describing functional dependencies of critical layer thickness and material parameters. We establish such relations here, in parts resorting to semi-empirical approximations in the interest of simplicity. Following our description of the FEA computations in Sect. 2.3., we may expect the pertinent tensile stresses to be comprised of a complex mixture of bulk laminate and individual sublayer flexural stresses, plus near-surface contact stresses. We defer detailed consideration of these competing stress components to an Appendix, focussing in this section on essential results only.

First, establish a reference state by defining the critical load P_D for radial cracking in a monolithic brittle coating of thickness D and Young's modulus E_c on an infinitely thick soft substrate of modulus E_s , corresponding to the condition where the maximum flexural tensile stress at the coating undersurface equals the strength σ_F of the material. Solutions for the stresses in bilayer systems of this kind may be obtained from the theory of thick plates on elastic foundations [21]. In earlier studies on such structures subjected to point-contact loading [1,2,4] we made use of these solutions to derive a critical load relation

$$P_D = B\sigma_F D^2 / \log(CE_c/E_s) \quad (1)$$

with dimensionless coefficients $B=1.35$ and $C=1$ [22]. Although it is implicit in Eq. (1) that the stress field leading to Eq. (1) is essentially flexural

(characteristic $\sigma \propto P/D^2$ dependence), we may recall from Figs. 4 and 5 that contact stresses will continue to dominate at and near the top surface.

Now consider a multilayer of n brittle layers of modulus E_i and thickness $d=D/n$ interspersed with compliant interlayers of modulus E_i and thickness h (Fig. 1). Generally, our goal is to determine relative critical applied loads P_1, P_2, \dots, P_n for any given set of parameters—specifically $n, h/d, E_i/E_c$ and E_s/E_c . However, because the tensile hoop stresses responsible for radial cracking are expected to have peak values in either the top or bottom layers (depending on the laminate parameters—Sect. 2.3.), we focus in this section on critical loads P_1 and P_n . Noting our conclusion from the FEA case studies in Figs. 4 and 5 that thin soft interlayers are unlikely to have much effect on the stress state at the undersurface of the n^{th} layer, the critical load for this layer may reasonably be approximated by

$$P_n = P_D \quad (2)$$

Determination of P_1 is less straightforward. In analogy to Eq. (1), define a quantity P_d for a single brittle layer of thickness d and modulus E_c on an infinitely thick substrate of compliant interlayer of modulus E_i

$$P_d = B\sigma_F d^2 / \log(CE_c/E_i) \quad (3)$$

In laminates, the thickness h of the interlayer is finite, with at least one brittle support layer of thickness d beneath, reducing flexure of the first layer—thus, P_1 must generally be somewhat higher than P_d . The functional dependence of P_1 on h/d for an analogous system with top glass plate and underlying interlayer, but on an infinitely thick brittle support layer, has been empirically determined to be of the form [2]

$$P_1/P_d = f_1 = 1 + \beta(d/h)^\gamma \quad (4)$$

where β and γ are data-adjusted coefficients for a given material system (Appendix). (Note that P_1 reduces to P_d in the limit $h \gg d$, as required.) This dependence may be anticipated to remain a reasonable approximation in the uppermost layers of laminate structures, especially when n is large. Strictly, we may expect f_1 to depend modestly on modulus ratios as well, i.e. $f_1 =$

$f_1(h/d, E_c/E_i, E_c/E_s)$, but we ignore such complications here. Combining Eqs. (1)–(4), we obtain the following expression

$$P_1/P_D = (1/n^2)[1 + \beta(d/h)^\gamma][\log(CE_c/E_s)/\log(CE_c/E_i)] \quad (5)$$

Eq. (5) conveniently separates the influence of number of layers, thickness ratio, and modulus ratios.

As demonstrated in the Appendix, incorporation of contact and bulk laminate flexure terms in the stress analysis allows for the determination of a more accurate (but unwieldy) relation for P_1/P_D than Eq. (5), especially for small n and h/d and E_i/E_c approaching unity. Analogous (unwieldy) relations for critical loads P_i/P_D in the intermediate layers ($i=2, 3, \dots, n$) are similarly determined in the Appendix.

In terms of the above analytical relations, the optimum condition for success of the multilayer is that $P_1/P_n \geq 1$.

5. Predictions for selected multilayer systems

We are now in a position to test the validity of the closed-form solutions derived in the preceding section. To do this we compare with FEA-generated data for hypothetical multilayer systems, making use of the algorithm described in Sect. 2.3. We retain some input parameters pertinent to the experimental systems in Sect. 3.: *brittle glass layers*, thickness $d=1.0$ mm, elastic constants $E_c=70$ GPa and $\nu_c=0.22$; *polycarbonate substrates*, $E_s=2.35$ GPa and $\nu_s=0.41$. Other parameters are allowed to vary: *bonding interlayers*, thickness h and modulus E_i (but fixed $\nu_i=0.25$). Also, we now consider a WC indenting sphere of small radius $r=0.5$ mm, to approximate more closely the point-load contact conditions inherent in Eq. (5). Analysis is carried out for up to $n=10$ layers. In the examples below (Figs. 8–11), data points are FEA calculations, solid curves are from Eq. (5), and dashed curves are from the more accurate relation Eq. A5 in the Appendix (recalling that only integer values of n are meaningful in these functional predictions).

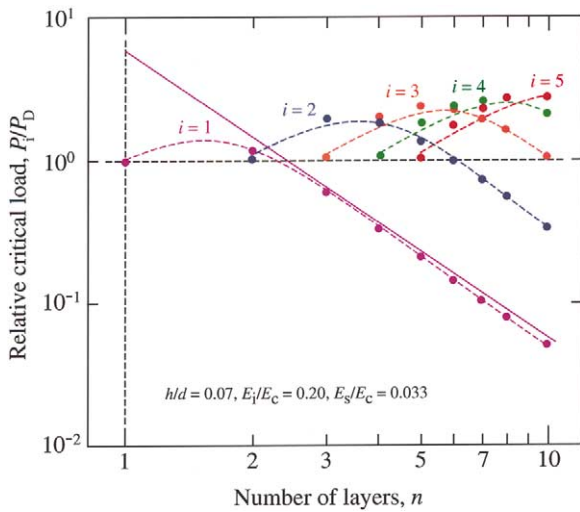


Fig. 8. Critical loads P_i/P_D , as function of number of layers n , for given multilayer system ($h/d=0.070$, $E_i/E_c=0.20$, $E_s/E_c=0.033$). Data points are FEA predictions. Dashed curves are best fits to data for all P_i/P_D , from Eq. A5. Solid line is asymptotic limit to P_i/P_D data from Eq. (5).

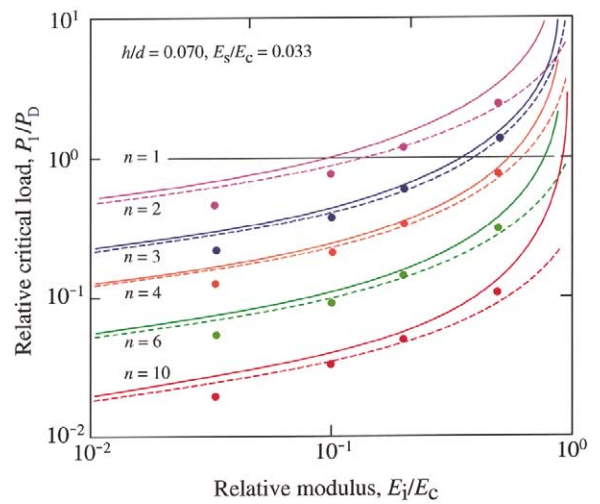


Fig. 10. Critical loads P_i/P_D as function of relative interlayer modulus E_i/E_c , for values of n indicated ($h/d=0.070$, $E_s/E_c=0.033$). Data points are FEA predictions. Solid curves are predictions from Eq. (5), dashed curves are more accurate predictions from Eq. A5.

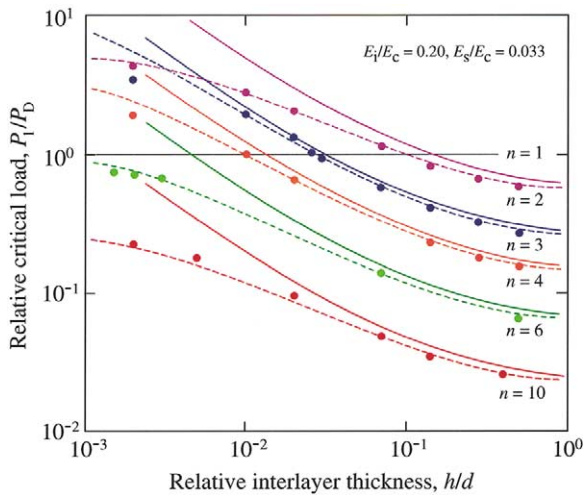


Fig. 9. Critical loads P_i/P_D as function of relative interlayer thickness h/d , for values of n indicated ($E_i/E_c=0.20$, $E_s/E_c=0.033$). Data points are FEA predictions. Dashed curves are best fits to data using Eq. A5, solid curves are evaluations from Eq. (5).

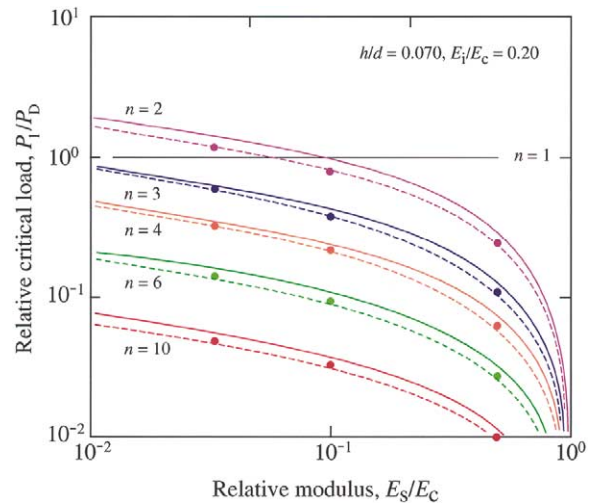


Fig. 11. Critical loads P_i/P_D as function of relative substrate modulus E_s/E_c , for values of n indicated ($h/d=0.070$, $E_i/E_c=0.20$). Data points are FEA predictions. Solid curves are predictions from Eq. (5), dashed curves are more accurate predictions from Eq. A5.

To investigate the role of number of layers, consider a laminate with n interlayers of modulus $E_i=14$ GPa ($E_i/E_c=0.20$) and thickness $h=70$ μm ($h/d=0.070$), bonded to the prescribed substrate

material ($E_s/E_c=0.033$). Fig. 8 plots relative critical loads P_i/P_D to produce cracks in each i^{th} layer ($i=1, 2, 3, \dots, n$) as a function of n . Our primary interest is in the P_i/P_D function for top layer radial crack-

ing ($i=1$). In this plot, the FEA data for $P_1(n)$ are best-fitted to Eq. A5 (dashed curves), yielding $f_1=2.68$. At large n , the FEA data tend asymptotically to the predicted n^2 dependence in Eq. (5) (solid line). At small n , the P_1 data show increasing deviation from this dependence, with limiting value close to unity at $n=1$ (monolith).

Also included in Fig. 8 are FEA data for P_1/P_D ($i=2, 3, 4, \dots$) and corresponding functional fits to Eq. A5 from the Appendix (dashed curves). For any given n (except the special case $n=2$), the critical load P_1 is lower than all P_2, P_3, P_4, \dots , confirming the dominance of top layer fracture for this particular multilayer configuration. Note that the FEA data points for P_n/P_D ($i=n$) lie close to unity, in accordance with Eq. (2). This confirms that the critical load at the multilaminate undersurface is not strongly dependent on the presence of intervening adhesive layers (at least not for the relatively small $h/d=0.070$ used here), i.e. the bulk laminate behaves as an equivalent monolith of thickness $D=nd$.

Fig. 9 shows the effect of relative adhesive thickness h/d on top layer critical load P_1/P_D , for various n , for fixed modulus ratios ($E_i/E_c=0.20$, $E_s/E_c=0.033$). Best fits of Eq. A5 to the FEA data yield parameters $\beta=0.18$ and $\gamma=0.84$ in Eq. (4) (consistent with $f_1=2.68$ from the calibration in Fig. 8). For any given n , P_1/P_D decreases monotonically with h/d , demonstrating the increasing facility for top-layer flexure with increasing interlayer thickness. The falloff in P_1/P with n from curve to curve is consistent with the n^2 dependence in Eq. (5). Note that predictions from the simplistic Eq. (5) (solid curves) are able to describe broader trends in the FEA data, but show marked deviations in the regions of small h/d and n —whereas Eq. (5) predicts $P_1/P_D \rightarrow \infty$ as $h \rightarrow 0$, Eq. A5 predicts finite limits, in accordance with the FEA data. These latter deviations are attributable to the dominance of top layer contact stresses (Appendix), neglected in Eq. (5).

Fig. 10 shows the effect of interlayer modulus mismatch E_i/E_c on P_1/P_D for various n , for fixed relative interlayer thickness and substrate modulus ($h/d=0.070$, $E_s/E_c=0.033$), now using the calibrated β and γ values from Fig. 9 to generate the curves. For any given n , P_1/P_D increases monotonically

with E_i/E_c , with increasing rapidity at $E_i/E_c \rightarrow 1$ (monolith limit). This plot demonstrates the enhancing influence of a more compliant interlayer (lower E_i/E_c) on radial cracking. Once more, the falloff in P_1/P_D values from curve to curve reflects the n^2 dependence in Eq. (5); and better fits to the FEA data are obtained with Eq. A5 (dashed curve) than with Eq. (5) (solid line), most noticeably in the regions of large E_i/E_c .

Fig. 11 shows the effect of substrate modulus mismatch E_s/E_c on P_1/P_D for various n , and for fixed relative interlayer thickness and interlayer modulus ($h/d=0.070$, $E_i/E_c=0.20$), again using the calibrated values of β and γ . For a given n , P_1/P_D decreases monotonically with E_s/E_c , with rapid falloff at $E_s/E_c \rightarrow 1$ (monolith limit). In this case, a stiffer substrate (higher E_s/E_c) diminishes the relative critical load for radial cracking, because P_D in Eq. (1) tends to infinity. The same curve-to-curve n^{-2} dependence in Eq. (5) is yet again apparent; and the dashed curves once more provide better approximations to the FEA data.

As foreshadowed at the end of the last section, one feature of the results in Figs. 8–11 bears special consideration. Certain configurations exist that satisfy the requirement $P_1/P_n \geq 1$ for multilayers to outperform their monolithic counterparts. We can determine these configurations from the results in such figures and thence construct design maps for specified systems. By way of illustration, suppose that we are asked to assemble a multilayer system from given glass layers and polycarbonate substrates ($E_s/E_c=0.033$), but that we are free to choose the bonding interlayer material. What combinations of modulus and thickness will provide optimum resistance to the incidence of fracture? Fig. 12 plots $(E_i/E_c)_*$ as a function of (h/d) , for several n , with the asterisk corresponding to the optimal condition $P_1/P_n=1$. Individual points are interpolations from FEA data such as those in Figs. 9 and 10, solid curves are corresponding predictions from Eq. (5), dashed curves from Eq. A5. There are some deviations between the predicted curves and FEA points at small E_i/E_c (cf. Fig. 10), highlighting the dangers of extrapolating beyond the data range. For safe operation, it is necessary to remain above these curves. The combinations of

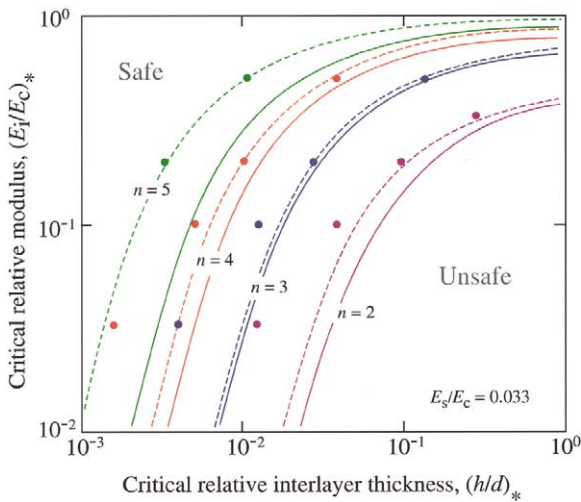


Fig. 12. Design diagram, showing optimal values $(E_i/E_c)_*$ as a function of $(h/d)_*$, for values of n indicated ($E_i/E_c=0.033$). Points are FEA data (interpolated from plots such as Figs. 9 and 10 at $P_1/P_D=1$), curves are corresponding predictions from Eq. (5) (solid) and Eq. A5 (dashed). To avoid premature radial cracking in upper layer, it is necessary to remain above these curves.

variables required to satisfy this condition may be readily determined from such design diagrams.

6. Discussion

We have investigated the conditions for fracture in laminates of brittle plates with compliant interlayers bonded to compliant substrates. Simple contact experiments on model glass/polycarbonate multilayer systems have been used to observe radial cracking at the brittle layer undersurfaces, and to measure corresponding critical loads for initiation. Generally, we find that cracking initiates first in either the top or bottom layer, depending on laminate modulus and thickness parameters. At first initiation, the cracks remain contained within individual layers until, at much higher loads, cracking occurs in all layers and system failure ensues. Spurious cone cracks may also occur at the laminate top surface, but these are considered unlikely to penetrate into the sublayers (except perhaps in very thin brittle plates), and are consequently of secondary importance.

Basic fracture mechanics relations have been derived to account for the critical loads for radial cracking in n -layer laminates of brittle layer thickness d and interlayer thickness h , with special attention to top- and bottom-layer loads P_1 and P_n . A central premise of the derivations is that the brittle layers flex on their soft interlayer and substrate supports, much as plates on elastic foundations in concentrated loading—the flexure generates undersurface tensile stresses which, in turn, generate radial cracks. This premise is best satisfied when n and h/d are large and the modulus ratio E_i/E_c is small. The load P_n is well approximated by P_D for a monolithic coating of equivalent thickness $D=nd$, Eq. (2). For load P_1 , an explicit but approximate and semi-empirical relation is determined, Eq. (5). A simplifying feature of Eq. (5) is that the principal variable dependencies appear as separable terms: for number of layers, as n^{-2} ; for interlayer thickness, as a power-law term in h/d ; for modulus dependence, as logarithmic terms in E_i/E_c , and E_s/E_c . A more accurate determination of P_1 , in which the stresses in the multilayer are broken down in terms of superposed bulk laminate and individual sublayer flexural components plus a near-surface contact component, provides a more accurate (but unwieldy, interactive) relation (Appendix, Eq. A5). These relations are able to account for all the important trends in independently generated FEA data for selected hypothetical multilayer systems in Figs. 8–11, although Eq. (5) becomes inaccurate in limiting regions (small n and h/d , E_i/E_c close to unity). Implicit in the P_1 relations, dependent as they are on dimensionless quantities (n , h/d , E_i/E_c and E_s/E_c), is a certain geometrical similarity, which holds only as long as the stresses in the system remain proportional to the applied load. Strictly, such linearity can only be realized in the limit of point contact (Boussinesq) loading, where the contact radius remains an insignificant fraction of the layer thickness d .

The fracture mechanics relations provide a sound basis for optimizing the design of brittle multilayer structures, by imposing a condition that radial cracking in the top layer occurs at a higher load than in the bottom layer, i.e. by ensuring $P_1/P_n \geq 1$. An example of a design diagram constructed on this basis was given in Fig. 12. Such

diagrams map out conditions under which the susceptibility to radial cracking of a multilayer system just equals that of an equivalent monolith. The requisites for falling within a safe domain for any given n is that h/d be kept sufficiently small and E_i/E_c sufficiently large—yet not to the extent that the multilayer begins to behave as a monolith, such that cracks are able to traverse the soft interlayers [18]. Ideally, therefore, one should design the system so as to lie as close as possible to the curves in Fig. 12.

In this study we have considered just layers and interlayers of the same kind and thickness, in the interest of simplicity. Other, more complex alternatives might be contemplated, in order to increase P_1 relative to P_D . For example, one might consider “strengthening” the top layer, e.g. by increasing the quantities d_1 or E_1 , or decreasing h_1 , relative to their sublayer counterparts. Again, it is important not to overdo any such strategy, in order that the damage tolerance properties of the multilayer not be compromised.

Acknowledgements

This study was supported by NIST internal funds and by a grant from the US National Institute of Dental Research.

Appendix. More detailed fracture mechanics analysis

Consider a laminate of brittle ceramic layers of Young’s modulus E_c with thin intervening compliant interlayers of modulus E_i , the whole bonded to a compliant substrate of modulus E_s , subject to a point-force load P at the top surface. Define a coordinate z_i along the contact axis locating the undersurface center of the i^{th} brittle layer. The net hoop stress at any such location may be approximated as the sum of three terms:

$$\sigma_i = (1-2\nu_c)P/4\pi z_i^2 + (2z_i/D-1)\sigma_0 + [(P/Bf_i z_i^2)\log(CE_c/E_i)], \quad (0 \leq z_i \leq D). \quad (\text{A1})$$

(i) *Contact load*. The first term represents an inverse-square Boussinesq point-force field (ν_c Poisson’s ratio) [23]. (ii) *Laminate flexure*. The second term represents flexure of the composite laminate on the substrate. This term is assumed to have a customary linear profile across the laminate section, with σ_0 the maximum value at $z=0$ and D . (iii) *Layer flexure*. The third term represents flexure of any individual brittle layer i on the compliant interlayer immediately beneath it. This term is obtained by rearranging Eqs. (3) and (4) in the text (replacing d by z_i), with f_i some function of i . It is implicit in Eq. A1 that the bulk of the load is supported by the stiff brittle layers, and that superposition of any one component does not distort the others.

The stress at the bulk laminate undersurface may be determined from the theory of plates on elastic foundations to be of the form [21]

$$\sigma_D = P \log(CE_c/E_s)/BD^2 \quad (\text{A2})$$

(which reduces to Eq. (1) in the text at $\sigma_D=\sigma_F$, $P=P_D$). Inserting $\sigma_i=\sigma_D$ at $z=D$ as a boundary condition in Eq. A1 and defining $z_i=id=in$, we may eliminate σ_0 to obtain

$$\sigma_i = (P/BD^2)(n/i)^2 \{ (1-2\nu_c)B(1-\mu)/4\pi + \mu \log(CE_c/E_s) + (1/f_i - \mu/f_n) \log(CE_c/E_i) \}, \quad (1 \leq i \leq n) \quad (\text{A3})$$

where $f_i=f_n$ at $i=n$ and

$$\mu = (i/n)^2(2i/n-1) \quad (\text{A4})$$

Note limiting values $\mu=1$ at $i=n$, $\mu \rightarrow 0$ at $i \ll n$.

The relative critical load analogous to Eq. (5) in the text is obtained by combining Eq. A3 with A2:

$$P_i/P_D = (i/n)^2 \log(CE_c/E_s) / \{ (1-2\nu_c)B(1-\mu)/4\pi + \mu \log(CE_c/E_s) + (1/f_i - \mu/f_n) \log(CE_c/E_i) \}, \quad (1 \leq i \leq n) \quad (\text{A5})$$

This equation reduces to Eq. (5) in the text at $i=1$ in the limit $n \gg 1$, $E_i/E_c \ll 1$. The term f_i can be adjusted to match FEA-generated P_i/P_D data. In

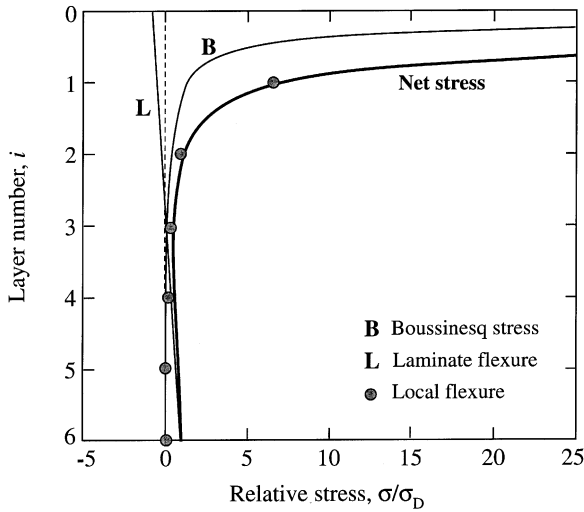


Fig. 13. Plot of tensile hoop stresses σ/σ_D as function of z/h along point-contact axis. Showing contributions to combined net stress from bulk laminate flexure, individual layer flexure (integer i only), and contact ($r=0.5$ mm). Calculations for $n=6$, $h/d=0.070$, $E_i/E_c=0.20$, and $E_s/E_c=0.033$. Local layer flexure term dominates in top layer, laminate flexure term dominates in bottom layer.

conjunction with the definition of f_i in Eq. (4), it is found that the empirical relation

$$f_i = f_1 i^{0.67} \quad (\text{A6})$$

provides a reasonable fit to the data in Fig. 8.

Fig. 13 plots each of the terms in Eq. A3, for a glass/polycarbonate system with $n=6$ layers. The local flexure term dominates at $i \ll n$, the bulk flexure term at $i \rightarrow n$. The Boussinesq term becomes important relative to the local flexure term when $h/d \rightarrow 0$. Radial cracking occurs in layer i when σ_i equals the bulk strength σ_F of the brittle layer material.

References

- [1] Chai H, Lawn BR, Wuttiaphan S. J. Mater. Res. 1999;14:3805.
- [2] Chai H, Lawn BR. J. Mater. Res. 2000;15:1017.
- [3] Lawn BR, Lee KS, Chai H, Pajares A, Kim DK, Wuttiaphan S, Peterson IM, Hu X. Advanced Eng. Mater. 2000;2:745.
- [4] Rhee Y-W, Kim H-W, Deng Y, Lawn BR. J. Am. Ceram. Soc. 2001;18:1066.
- [5] Miranda P, Pajares A, Guiberteau F, Cumbrera FL, Lawn BR. J. Mater. Res. 2001;16:115.
- [6] Kelly JR. Ann. Rev. Mater. Sci. 1997;27:443.
- [7] Lawn BR, Deng Y, Thompson VP. J. Prosthet. Dent. 2001;86:495.
- [8] Eberhardt AW, Lewis JL, Keer LM. ASME J. Biomed. Eng. 1991;113:410.
- [9] Ball A. J. de Physique IV 1997;7:C3921.
- [10] Grant PV, Cantwell WJ, McKenzie H, Corkhill P. Inter. J. Impact Eng. 1998;21:737.
- [11] Grant PV, Cantwell WJ. J. Testing and Eval. 1999;27:177.
- [12] Bennison SJ, Jagota A, Smith CA. J. Am. Ceram. Soc. 1999;82:1761.
- [13] Maekawa I, Sudou H, Uda K. Inter. J. Impact Eng. 2000;24:673.
- [14] Pawlowski L. The science and engineering of thermal spray coatings. New York: John Wiley, 1995.
- [15] Bushan B. Tribology and mechanics of magnetic storage devices. 2nd ed. New York: Springer-Verlag, 1996.
- [16] Marshall DB. Am. Ceram. Soc. Bull. 1992;71:969.
- [17] Liu H, Lawn BR, Hsu SM. J. Am. Ceram. Soc. 1996;79:1009.
- [18] Shaw MC, Marshall DB, Dadkhah MS, Evans AG. Acta Metall. 1993;41:3311.
- [19] Jorgensen O, Horsewell A. Acta Metal. 1997;8:3431.
- [20] Fischer-Cripps AC, Lawn BR, Pajares A, Wei L. J. Am. Ceram. Soc. 1996;79:2619.
- [21] Timoshenko S, Woinowsky-Krieger S. Theory of Plates and Shells. 2nd ed. New York: McGraw-Hill, 1959.
- [22] Kim H-W, Deng Y, Miranda P, Pajares A, Kim DK, Kim H-E, Lawn BR. J. Am. Ceram. Soc. 2001;84:2377.
- [23] Timoshenko S, Goodier JN. Theory of Elasticity. 2nd ed. New York: McGraw-Hill, 1951.